PROTEINS: Structure, Function, and Genetics 29:321–333 (1997)

Solution Structure of Maurotoxin, a Scorpion Toxin From *Scorpio maurus*, With High Affinity for Voltage-Gated Potassium Channels

E. Blanc,[1] J.M. Sabatier,[2] R. Kharrat,[3] S. Meunier,[1] M. El Ayeb,[3] J. Van Rietschoten,[2] and H. Darbon[1]*
[1]*AFMB, CNRS UPR 9039, IFR1, Marseille, France*
[2]*CNRS URA 1455-IFR Jean-Roche, Faculté de Médecine-Nord, Bd. Pierre-Dramard, Marseille, France*
[3]*Laboratoire des Venins et Toxines, Institut Pasteur de Tunis, Tunis-Bélvédère, Tunisie*

ABSTRACT **Maurotoxin (MTX), purified from the scorpionid *Scorpio maurus* is a potent ligand for potassium channels. It shows a broad specificity as being active on Kv1.1 (Kd = 37 nM), Kv1.2 (Kd = 0.8 nM), Kv1.3 (Kd = 150 nM) voltage-gated potassium channels, as well as on small-conductance calcium-activated potassium channels. It has a unique disulfide pairing among the scorpion toxins family. The solution structure of MTX has been determined by 2D-NMR techniques, which led to the full description of its 3D conformation: a bended helix from residues 6 to 16 connected by a loop to a two-stranded antiparallel β sheet (residues 23 to 26 and 28 to 31). The interaction of MTX with the pore region of the Kv1.2 potassium channel has been modeled according to their charge anisotropy. The structure of MTX is similar to other short scorpion toxins despite its peculiar disulfide pairing. Its interaction with the Kv1.2 channel involves a dipole moment, which guides and orients the toxin onto the pore, toward the binding site, and which thus is responsible for the specificity. Proteins 29:321–333, 1997.** © 1997 Wiley-Liss, Inc.

Key words: scorpion neurotoxin; NMR; structure; potassium channel; maurotoxin

INTRODUCTION

Potassium channels form a family of proteins with varied modes of activation and regulation, since they are involved in divers biological processes.[1,2] Scorpion neurotoxins are potent ligands for these proteins and form a structurally related family of proteins, divided into two classes, depending on their length. The so-called short neurotoxins (<40 residues) are active on potassium channels,[3–10] whereas the long ones (60–70 amino acid residues long) are, to our best knowledge, specific for sodium channels.[11,12] The specificity of short neurotoxins for the various potassium channels has been investigated, through the generation of mutants of both receptors and toxins,[13–15] which led to a description of the interaction surface between charybdotoxin (CTX) and large conductance potassium channels (BK),[15] as well as between kaliotoxin (KTX) and the Kv1.3 potassium channel.[16]

Noxiustoxin (NTX) is the first described scorpion toxin ligand, specific for potassium channels,[17] and since then, several others have been described, all coming, until recently, from buthid venoms. However, it has recently been demonstrated that the scorpionid *Scorpio maurus* also possesses potassium channel ligands. One of them, namely, maurotoxin (MTX) has been purified and characterized.[58] It is a blocker of the voltage-gated potassium channels Kv1.1 (Kd = 37 nM), Kv1.2 (Kd = 0.8 nM), Kv1.3 (Kd = 150 nM) and competes with radioiodinated apamin for the binding to small conductance calcium-activated apamin-sensitive potassium channels (SK) with a $K_{0.5}$ = 5 nM. The primary structure of MTX (34 amino acid residues) is highly homologous to other related toxins (Fig. 1), but MTX is reticulated by four disulfide bridges, instead of three, for all but one (Pi1 from *Pandinus imperator*[18] short scorpion toxins). Previous studies have demonstrated that the disulfide pairing of MTX is atypical when compared with other toxins, including Pi1.[58,59]

In this paper, we describe the three-dimensional solution structure of synthetic MTX (sMTX), determined by ^{1}H-2D NMR techniques and compare the obtained results with related toxins of known structures, such as NTX,[19] CTX,[20] agitoxin 2 (AgTX2),[21] KTX,[16] and margatoxin (MgTX).[22] We demonstrate that, despite the atypical disulfide pattern, the sMTX adopts the alpha/beta scorpion toxin scaffold. We also investigate the electrostatic characteristics of sMTX, and propose a model of interaction with the voltage-gated potassium channel Kv1.2.

The pdb coordinate files are available on the web site http://afmb.cnrs-mrs.fr/subjects/maurotoxin, and have been deposited on the Brookhaven Data Bank (PDB Ident code 1txm).

S. Meunier's present address: Bijvoet Center for Biomdescher Research, Dept. of Chemistry, Utrech University, 358h Utrecht, The Netherlands.

*Correspondence to: Dr. H. Darbon, AFMB-UPR 9039, CNRS IFR1, Chemin Joseph-Aiguier, 13402 Marseille CEDEX 20, France.

Received 19 November 1996; Accepted 22 November 1996

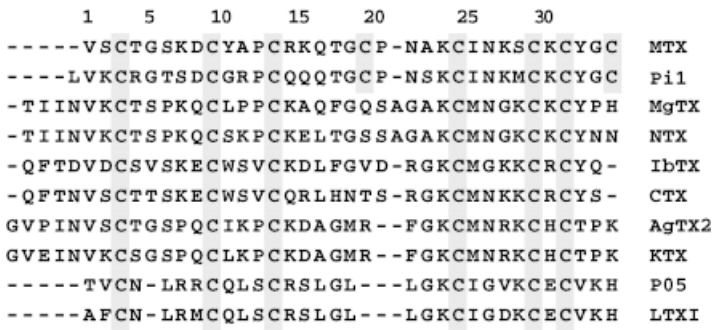

Fig. 1. Amino-acid sequence of maurotoxin aligned with other related scorpion toxins: Pi1,[18] margatoxin (MgTX),[3] noxiustoxin (NTX),[4] iberiotoxin (IbTX),[5] charybdotoxin (CTX),[6] agitoxin 2 (AgTX 2),[7] kaliotoxin (KTX),[8] P05,[9] and leiurotoxin I (LTXI).[10]

MATERIALS AND METHODS

Sample Preparation

The synthesis of MTX by solid-phase synthesis has been described elsewhere.[59] We dissolved 8 mg of purified peptide in 0.5 ml of H_2O/D_2O (90/10 v/v), pH 3 uncorrected for isotope effects, leading to a concentration of 2 mM. Amide proton exchange rate was determined after lyophilization and dissolution in 100% D_2O.

NMR Spectroscopy

All ^1H NMR spectra were recorded on a BRUKER DRX 500 spectrometer. The experiments were performed at 290 and 300 K in order to solve assignment ambiguities. At 300 K, a double-quantum-filtered two-dimensional correlation spectrum (DQF-COSY)[23,24] was acquired in the phase-sensitive mode [1024 (t1) $\times$ 4096 (t2) complex data points], by time-proportional phase incrementation (TPPI) of the first pulse.[25] A clean total correlation spectroscopy (TOCSY)[26,27] (80 ms spin lock), and phase-sensitive two-dimensional nuclear Overhauser effect spectra (NOESY)[28] (mixing time of 80 ms) were recorded with 750 (t1) $\times$ 2048 (t2) complex data points. At 290 K, a DQF-COSY [1024 (t1) $\times$ 4096 (t2) complex data points], a clean TOCSY (2048 $\times$ 512) with a spin lock of 80 ms, and a NOESY (2048 $\times$ 512) were acquired. The amide proton exchange experiments were recorded immediately after dissolution of the peptide in D_2O. Five NOESY spectra with mixing times of 80 ms were recorded at 290 K, the first one during a time period of 1 hour (1024 complex points with 256 experiments), followed by four spectra of 10 hours (1024 complex points with 512 experiments).

Data Processing

All data were processed using the NMRPipe software,[29] running on Silicon Graphic Indy R4400 and HP 9000 workstations. A linear prediction was applied in the first dimension. The matrices were transformed with a zero filling to the next power of 2 in the acquisition dimension, and to 1024 points in the other. The signal was multiplied by a shifted sine-bell window, in both dimensions, prior to a Fourier transform, and a fifth-order polynomial baseline correction was applied.

Spectral Analysis

The identification of amino acid spin systems and the sequential assignment were done by using the standard strategy described by Wüthrich.[30] The comparative analysis of COSY and TOCSY spectra recorded in water gave the spin systems signature of the protein. The spin systems were sequentially connected by using the NOESY spectra.

Experimental Restraints

The integration of nuclear Overhauser enhancement (nOe) data was done using lineshape integration routine of the EASY software,[31] running on a SUN-IPC workstation. On the basis of known distances in regular secondary structures ($d_{H\alpha-H\alpha}$ = 2.3 Å and d_{HN-HN} = 3.3 Å between two strands of an antiparallel β sheet, $d_{H\alpha-HN}(i, i + 3)$ = 3.4 Å $d_{H\alpha-HN}(i, i + 4)$ = 4.2 Å $d_{HN-HN}(i, i + 1)$ = 2.8 Å in α helix) the intraresidue and sequential peaks were divided into four categories according to their relative intensities; that is, strong $<$2.4 Å, medium $<$2.9 Å, weak $<$3.5 Å, and very weak $<$5.0 Å. The medium- and long-range nOe's were divided into two classes, depending on whether they occurred between two backbone protons ($<$4 Å) or not ($<$5 Å). The lower limits were systematically set at 1.8 Å.

The ϕ torsion angles constraints resulted from the $^3J_{HN-H\alpha}$ coupling constant measurements. They were divided, according to Wüthrich[30] into small ($<$7 Hz) and large ($>$7.7 Hz) angle restraints and, respectively, translated into $-55° \pm 15°$ and $-120° \pm 50°$.

The stereospecific assignment was made by using the HABAS routine of the DIANA[32] software, on the basis of the upper limits restraints and $^3J_{HN-H\alpha}$ $^3J_{H\alpha-H\beta2}$, $^3J_{H\alpha-H\beta3}$, and the GLOMSA routine of the DIANA software during refinement, using a set of preliminary structures. Pseudoatom corrections were

added when stereospecific assignments could not be obtained.

Structure Calculations

Distance geometry calculations were performed with the variable target function program DIANA 2.8.[32]

A preliminary set of 1000 structures was initiated, including only intraresidual and sequential upper limit distances. From these, the 500 best were kept for a second round, including medium-range distances, and the resulting 250 best for a third one, with the whole set of upper limits restraints, and some additional distance restraints, used to define the disulfide bridges (i.e., dSG,SG 2.1 Å, dCB,SG and dSG,CB 3.1 Å). Starting from the 50 best structures, a REDAC strategy[33] was used in a last step, in order to include the dihedral constraints together with the additional distances restraints coming from hydrogen bonds.

These 50 structures were then energy minimized over 10,000 iterations of the Powell algorithm of the XPLOR 3.1 package[34] using the AMBER force field (parameter files parmallh6x.pro and topallh3x.pro.).

Electrostatic Calculations

The dipole moments together with the electrostatic calculations and analysis were done by using the GRASP software[35] running on Silicon Graphics Workstations. The potential maps were calculated with a simplified Poisson-Boltzmann solver,[36] on the basis of an AMBER-derived parameter file.

The visual analysis of resulting structures and docking models were carried out with the TURBO-FRODO graphic software[37] running on Silicon Graphics workstations.

The analysis of the quality of the structures were done using the PROCHECK 3.3 and PROCHECK-NMR softwares.[38]

RESULTS

Sequential Assignment

The sequence-specific assignment was done following the standard method of Wüthrich.[30] The spin systems were identified on the basis of both COSY and TOCSY spectra, recorded in water at 300 and 290 K.

The use of two temperatures for recording allowed us to resolve overlapping signals in the fingerprint region, and thus, intraresidue HN–Hα cross peaks were unambiguously assigned. Starting from them, each spin system was characterized by its connectivities in the COSY and checked in the TOCSY spectra. Few methylene groups have only one resonance, due to either strict degeneracy or uncertainty in overcrowded regions.

The sequential connectivities were obtained from NOESY spectra, recorded in water at both 300 and 290 K, with a mixing time of 80 ms. The single isoleucine, I25, was taken as the starting point. The Hα–HN, HN–HN pathways are illustrated in Figure 2 and summarized in Figures 3 and 4. From I25, it has been possible to connect the polypeptide chain up to C34 and down to P20, using Hα–HN connections (Hβ–HN and/or HN–HN were present to confirm each assumption). A Hα–Hδ with an AMX spin system allowed us to assign it as C19 (confirmed by a HN–Hδ connection). Next, we used the remaining alanine, assigned as A11, as starting point to run down to D8 by virtue of strong HN–HN peaks (all confirmed by either a Hα–HN and/or Hβ–HN peak) and up to K15 by the use of a HN–Hδ peak with P12, and the combined use of HN–HN, Hα–HN, and Hβ–HN connections. From the remaining valine, assigned as V1, we connected the six first residues, and from the Q16 the sequence from 15 to 19 was constructed. The last step was to connect the last unassigned spin system, K7, to both S6 and D8. At the end of this procedure, all spin systems were unambiguously assigned (Table I).

Secondary Structure

The qualitative analysis of sequential nOe intensities, together with the pattern of medium range constraints allowed us to predict an helical conformation between S6 and Q16. There are, in this part of the protein, some strong sequential HN–HN, weak or inexistant Hα–HN and a stretch of medium range nOe's. We detected, still on the basis of this qualitative analysis, an extended fragment from N21 to I25, on one hand, and S28 to C31 on the other (strong Hα–HN together with weak HN–HN sequential nOe's). These two strands are connected by a tight turn centred on N26 and K27. A last fragment, the N-terminal one, is in extended conformation, from V1 to T4. Another predictive method was applied, developed by Wishart,[39] and based on the upfield/downfield shifts observed in β sheets/helices for the Hα chemical shifts. Applied to the sMTX, the secondary structures are the same as above, except for Y10 which has a chemical shift consistent with a β sheet (Fig. 3).

Coupling Constants

We measured 22 $^3J_{HN-H\alpha}$ coupling constants on NOESY spectra using the infit software.[40] We also measured 36 $^3J_{H\alpha-H\beta}$ on COSY maps, either directly (trivial spin systems) or by comparing them with a simulated pattern.[41] The $^3J_{HN-H\alpha}$ coupling constants were converted into ϕ-angle restraints according to their values. The ψ- and χ_1-angle restraints were generated by the HABAS routine of the DIANA software,[32] on the basis of the measured coupling constants and the determined distance restraints.

Hydrogen Bonds

We measured the exchange rate of amide protons with the solvent. The amide protons still present after 70 hours of exchange were considered as being engaged in hydrogen bonds. Most of them occurred

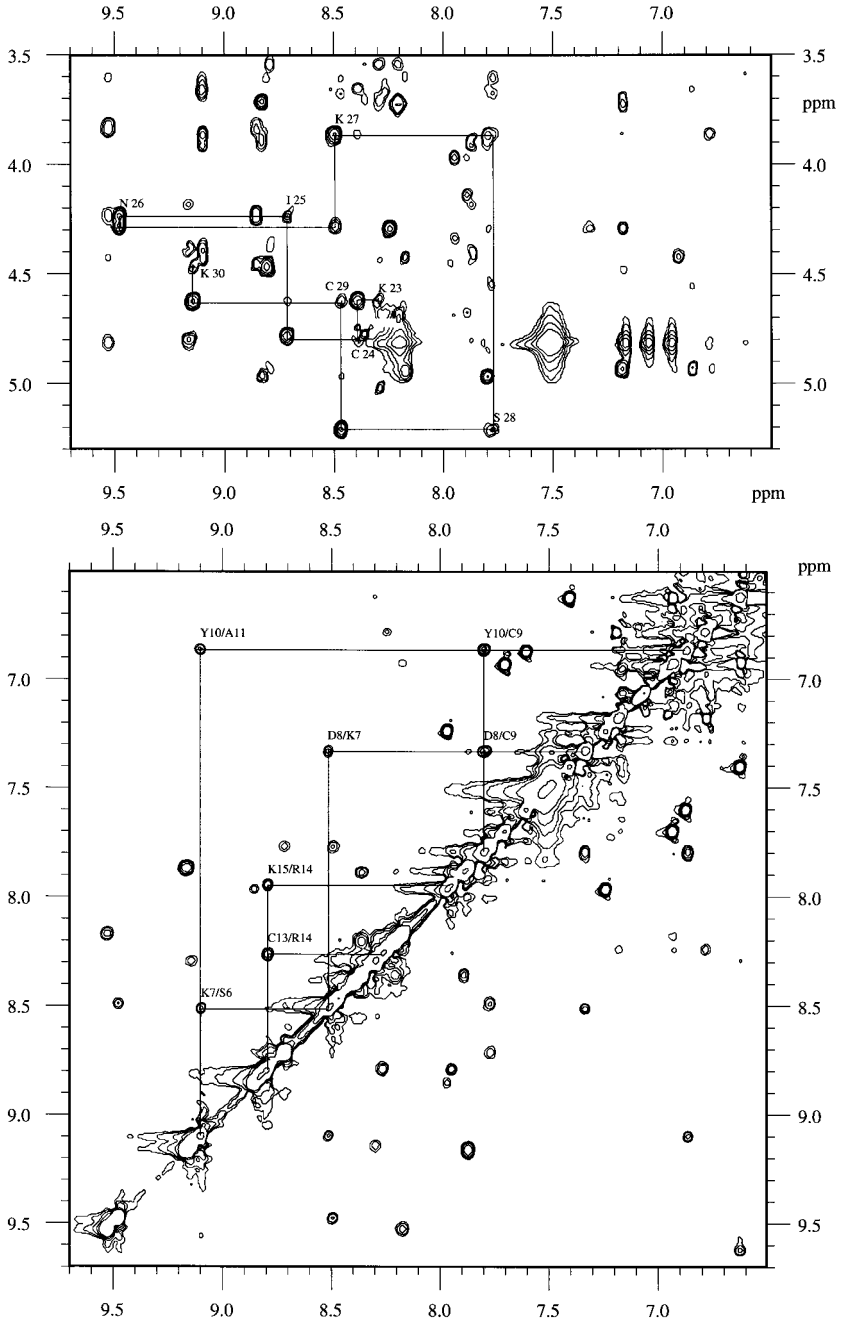

Fig. 2. Contour plots of a NOESY spectrum. **Top:** Fingerprint region. **Bottom:** Amide proton region. In both, some sequential connectivities are illustrated by lines.

in the regular structures. The amide proton partners were identified on the basis of the DIANA predictions for residues Y10, C13, R14, Q16, T17, and K30 in a first round, K23, I25 in a second round, and on the basis of the visual analysis for residues C3, C9, K15, G18, and S28 (Fig. 3).

Structure Calculations

The distance geometry calculations led to a single family of 50 structures exhibiting a target function comprised between 0.17 Å^2 and 1.07 Å^2. These 50 structures are all consistent with the experimental restraints, only seven distance violations greater than 0.2 Å (with a maximum of 0.31 Å) could be observed. Only one angle restraint is violated by more than 5° (6.15°).

The root-mean-square deviation (RMSD) of these 50 structures versus an average calculated one is 0.504 Å for the backbone atoms, and 0.999 Å for all the heavy atoms. The overall backbone geometry is

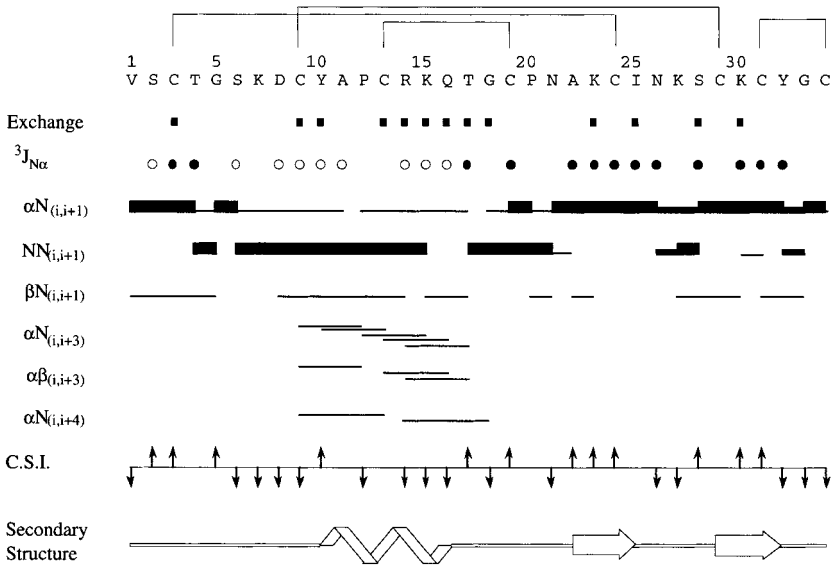

Fig. 3. Amino acid sequence of maurotoxin and a survey of NMR data used for locating the secondary structure elements: the sequential nOe's, extracted from NOESY with mixing times of 80 ms and classified as weak, medium, and strong, are represented by the thickness of the bars. Filled boxes indicate low amide proton exchange rates. Filled circles represent $^3J_{HN-H\alpha}$ coupling constants greater than 7.5 Hz and open circles those less than 7.0 Hz. The chemical shift indices (C.S.I.) of Hα protons are defined in ref. 39.

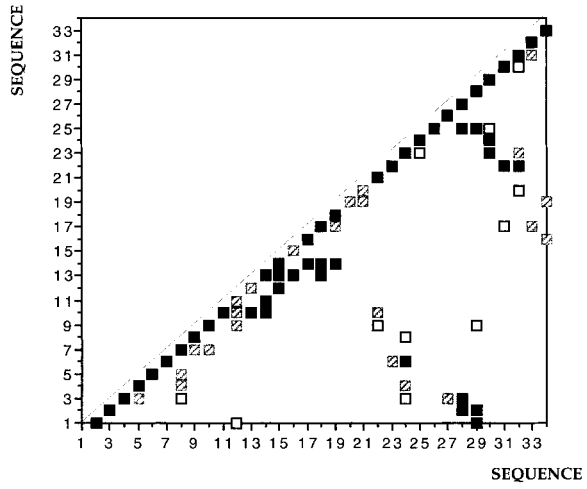

Fig. 4. Summary of nOe data. Filled square: An nOe between two backbone atoms. Shaded square: The nOe detected involves only one backbone atom. Open square: Both partners are side chain protons. When more than one nOe is detected between two residues, only the one involving the highest number of backbone atoms is indicated.

good, with a Ramachandran plot exhibiting 80% of the residues in the most favored regions, 19.2% and 0.8%, respectively, in additional and generously additional regions (according to the PROCHECK software nomenclature).

On the basis of these 50 structures, having some important nonbonded bad contacts, we started an energy minimization with the Powell algorithm of the XPLOR3.1 software.[34]

The final set of structures, composed of 35 structures presenting the best geometry, are of good quality, the negative Van der Waals energy indicates the absence of nonbonded contacts, and the correlation with the experimental restraints shows no distance violation greater than 0.2 Å, nor angle violation greater than 5°. The covalent geometry is respected as indicated by the low RMSD values on the bond lengths, and the valence angles (Table II). The analysis of the Ramachandran plot shows 69.7% of the residues in the most favored regions and 30.3% in the additional allowed regions (Fig. 5).

Structure Description

The calculated structures form a homogeneous family, sharing the same folding. The RMSD value of the 35 structures versus the average calculated one equals 0.470 Å for the backbone atoms and 0.960 Å for all heavy atoms. The backbone structure is well defined all along the sequence. The N-terminal segment is extended and the C-terminal loop is locked by a disulfide bridge. The other disulfide bridges connect the N-terminal part to the first strand of the β sheet, the helix to the second strand and the end of the helix to the following loop (Fig. 6).

The helix

The analysis of the structures, using TURBO-FRODO[37] and PROCHECK-NMR[38] indicates the presence of an α helix running from residue 6 to 16. However, not all the structures present this pattern, some of them have the helix shortened to a segment from 10 to 16. In fact, the helix possesses a proline

TABLE I. Chemical Shifts, Coupling Constants and Stereospecific Assignment of Maurotoxin at 290 K

		Chemical shift (ppm)				
Nature	Position	HN	Hα	Hβ	Others	$^3J_{HN-H\alpha}$ (Hz)
Val	1	8.201	3.716	1.959	$C_\gamma H_3$ 1.002	—
Ser	2	8.833	4.970	3.911, 3.874		5.9
Cys	3	7.801	4.806	2.998, 3.227		8.1
Thr	4	9.167	4.390	4.187	$C_\gamma H_3$ 1.142	9.7
Gly	5	7.874	4.423, 3.904			—
Ser	6	9.100	3.657	3.864		3.0
Lys	7	8.517	3.863	1.674	$C_\gamma H_2$ 1.596 $C_\delta H_2$ 1.273 $C_\epsilon H_2$ 2.918 $N_\epsilon H_2$ 7.524	
Asp	8	7.336	4.298	2.886,* 2.783		5.2
Cys	9	7.800	4.558	2.969, 2.664		6.9
Tyr	10	6.867	4.930	3.186,* 3.001		5.2
Ala	11	9.103	4.373	1.453		3.9
Pro	12		4.339	2.305, 1.816	$C_\gamma H_2$ 2.239,* 2.122 $C_\delta H_2$ 3.668,* 3.622	—
Cys	13	8.266	4.677	3.485, 2.999		—
Arg	14	8.794	3.547	1.876, 1.540	$C_\gamma H_2$ 1.348, 1.167 $C_\delta H_2$ 3.062, 3.137 NH_2 7.333	4.1
Lys	15	7.950	3.973	1.960, 1.864	$C_\gamma H_2$ 1.449, 1.394 $C_\delta H_2$ 1.644 $C_\epsilon H_2$ 2.924 $N_\epsilon H_2$ 7.534	4.6
Gln	16	7.893	4.140	2.192, 2.163	$C_\gamma H_2$ 2.493, 2.287 NH_2 7.238, 7.965	5.0
Thr	17	8.361	4.766	4.439	$C_\gamma H_3$ 1.198	9.8
Gly	18	8.208	3.707, 4.454			—
Cys	19	8.292	5.018	3.703, 2.057		7.6
Pro	20		4.485	1.816	$C_\gamma H_2$ 1.871, 1.720 $C_\delta H_2$ 3.742, 3.293	—
Asn	21	7.180	4.293	2.744, 2.790	NH_2 6.932, 7.704	—
Ala	22	8.245	5.352	1.412		8.7
Lys	23	8.301	4.620	1.808	$C_\gamma H_2$ 1.535, 1.384 $C_\delta H_2$ 1.723 $C_\epsilon H_2$ 2.938 $N_\epsilon H_2$ 7.481	7.7
Cys	24	8.392	4.799	2.756, 2.276		8.2
Ile	25	8.716	4.236	1.665	$C_\gamma H_2$ 1.355 $C_\gamma H_3$ 0.906 $C_\delta H_3$ 0.812	10.8
Asn	26	9.478	4.288	2.989, 2.672	NH_2 7.605, 6.873	8.8
Lys	27	8.495	3.867	2.210, 2.109	$C_\gamma H_2$ 1.347, 1.295 $C_\delta H_2$ 1.677, 1.617 $C_\epsilon H_2$ 2.950 $N_\epsilon H_2$ 7.492	—
Ser	28	7.772	5.208	3.677, 3.612		8.8
Cys	29	8.469	4.631	2.792, 2.443		—
Lys	30	9.144	4.467	1.769, 1.553	$C_\gamma H_2$ 0.989, 0.810 $C_\delta H_2$ 1.483 $C_\epsilon H_2$ 2.649, 2.818 $N_\epsilon H_2$ 7.486	10.3
Cys	31	8.809	4.949	2.522, 3.600		8.3
Tyr	32	8.176	4.424	2.381,* 3.197		8.0
Gly	33	9.527	4.236,* 3.833			
Cys	34	8.857	4.457	3.167, 2.793	NH_2 6.624, 7.407	—

*$H\alpha_1$, $H\beta_1$ $H\gamma_1$ or $H\delta_1$ when stereospecific assignment could be obtained.

TABLE II. Structural Statistics of the 35 Best Structures

	RMSD* (Å)	⟨DG⟩†	$\overline{DG}$‡
Backbone (C, Ca, N)	0.407		
All heavy atoms	0.960		
Energies (kcal/mol)			
Total		109.14 ± 8.40	97.01
Bonds		9.87 ± 1.01	8.29
Angles		93.31 ± 3.50	88.64
Improper		1.35 ± 0.16	1.20
van der Waals		−143.73 ± 3.89	−146.49
Dihedral		142.349 ± 1.35	141.35
nOe§		5.73 ± 0.88	3.73
Dihedral restraints§		0.25 ± 0.08	0.28
RMSD			
Bonds		0.0095 Å	0.0094 Å
Angles		2.54°	2.61°
Impropers		0.24°	0.25°

*The RMSD values are calculated with respect to the mean structure.
†⟨DG⟩ are the final 35 maurotoxin structures obtained by distance geometry and energy minimization.
‡$\overline{DG}$ is the mean structure obtained by averaging the coordinates of the individual DG structures best fitted to each other.
§The energy values for nOe and dihedral restraints are calculated with the same weighting function as geometric energies.

(P11) located in the middle of the helix. The resulting effect is a bending of the helix axis (38°). An (i, i + 4) hydrogen bond links G5 with C9, contrarily K7 is connected to Y10 by an (i, i + 3) hydrogen bond, characteristic of a 3_{10} helix. The ϕ–ψ values of the residue C9 shows that its conformation is closer to a 3_{10} helix conformation than to a classical α helix. Thus, the helix can be divided into two parts. The segment 10 to 16 presents a canonical α helix folding, while the segment 6 to 10 is more difficult to classify, since it is close to a 3_{10} helix conformation.

The β sheet

The previous analysis of the ϕ–ψ distribution also shows the presence of a two-stranded antiparallel β sheet. This β sheet, running from 22 to 25 and 28 to 31 is right-hand twisted and is stabilized by four hydrogen bonds. It is well defined as indicated by the RMSD value of the 35 structures versus the calculated average structure (0.247 Å) for the backbone between residues 23 and 31.

The two strands of the β sheet are connected by a turn formed by the residues N26 and K27. This turn is well defined and is a type I β turn.[42]

DISCUSSION

Comparison of Maurotoxin With Other Related Toxins

The sMTX adopts the classical scorpion toxin α-β scaffold (Fig. 7). Usually, this motif is stabilized by two disulfide bridges linking the helix to the β sheet.[43] Contrarily, the helix of sMTX is linked only by one disulfide bridge to the β sheet. The second bridge (which could be numbered C13–C31 in a regular pattern) is not present in sMTX, due to the particular disulfide pairing of this toxin. Thus, the new pairing does not disrupt the folding, even if some local changes appear, concerning the size of the β sheet. The β sheet has a length of three residues for each strand, which is to be compared to six residues in NTX[19] and MgTX[22] and five residues in the other short toxins (i.e., p05,[44] AgTX2,[21] CTX,[45] Iberiotoxin (IbTX),[46] p01[47]).

The type I turn N26-K27, connecting the two strands, is homologous both in sequence and structure to that of CTX (N30-K31, type I).[45]

The helix of sMTX is not a canonical α helix. We compared our results to those obtained for related toxins and observed, that such a bent structure had been previously described for other toxins, such as NTX, AgTX2, and MgTX. In fact the bending capacity of the helix is the result of the presence of a proline in position 12, and must be correlated with the existence of an alanine in position 22, instead of a glycine in most scorpion toxins. A consensus sequence for scorpion toxins was proposed, on the basis of the structural characterization of CTX and consists in C . . . CXXXC . . . GXC . . . CXC.[45] The authors considered the glycine as a conserved residue due to steric hindrance between the helix and the sheet.[45] The alpha/beta motif could not even accommodate the methyl side chain of an alanine. On the sight of the structure determination of NTX, MgTX, AgTX2, and sMTX, it appears that it exists an alternative to this consensus, which is C . . . CXXPC . . . AXC . . . CXC, where the methyl side chain of the alanine can now be inserted into the space, opened by the bent of the helix.

A last characteristic of sMTX must be highlightened: the N-terminal part is extended and well defined. The short scorpion toxins are all composed of a two or three stranded antiparallel β sheet. The sMTX, shorter than IbTX, CTX, NTX and MgTX, does not possess the third strand, located on the N-terminal fragment. Notwithstanding, the sMTX extremity (V1–T4) is structurally superposable to its equivalent in NTX (V5–T8), MgTX (V5–T8), AgTX2 (V6–T9) or CTX (V5–T8), showing a high degree of structural homology.

Disulfide Pairing

The disulfide pairing of the synthetic maurotoxin was determined using an enzymatic cleavage, followed by Edman degradation.[59] The proteolysis fragment analysis unambiguously identified the pattern C3–C24, C9–C29, C13–C19, C31–C34. Analysis of the native toxin Edman degradation also gave evidence for this pattern. This pairing is unique among the scorpion toxin family. We calculated the struc-

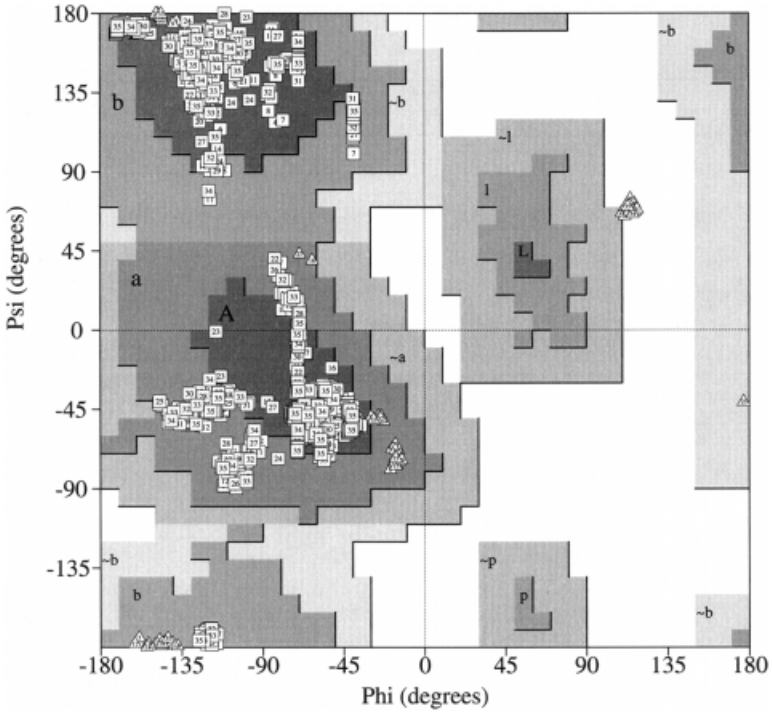

Fig. 5. Ramachandran plot[38] for the 35 best structures. The areas defined in dark gray are the most favored regions. The areas in light gray are the additional allowed regions. The glycines are shown as triangles. The numbers correspond to the structures, according to their quality, from the best to the worst.

ture of synthetic maurotoxin with these chemically determined disulfide bridges but we also performed a complete structure determination using the "standard" disulfide pairing, ie C3–C24, C9–C29, C13–C31, and C19–C34, to check for the conformational involvement of this nonclassical pattern. Indeed, the maurotoxin is the second short toxin with four disulfide bridges acting on K+ channels. The first to be characterized is Pi1,[18] from *Pandinus imperator* and it is highly homologous to the maurotoxin (71% of homology). The two toxins share the same specificity for voltage-dependent potassium channels. The sMTX is reticulated: 1st–5th, 2nd–6th, 3rd–4th, 7th–8th, whereas Pi1 is 1st–5th, 2nd–6th, 3rd–7th, 4th–8th. Unfortunately, the structure of Pi1 has not been published so far. Interestingly, we observed that the NMR derived dataset is compatible with both sets of pairing. The residual violations and the final energies of the structures calculated with a "standard" pattern are of the same order (Etot 100 kcal/mol, EnOe 4 kcal/mol, Ecdih 0.25 kcal/mol), and the structure quality, as judged from the ϕ–ψ distribution, is comparable. In fact, the two calculated structure families are highly homologous. The four sulfur atoms implicated in the two alternative disulfide bridges (C13–C19, C31–C34 or C13–C31, C19–C34) are all close to each other, within 6.5 Å. This may explain that the structure is not significantly affected by the switch from one pairing to the other.

Pharmacology

The sMTX is a toxin, active on voltage-gated potassium channels Kv1.1 (Kd = 37 nM), Kv1.2 (Kd = 0.8 nM) and Kv1.3 (Kd = 150 nM). Previous analysis of mutants of CTX and their relative binding to Shaker channels, allowed the identification of residues directly involved in the interaction of the toxin with a voltage-gated potassium channel.[48] Five residues, K27, M29, N30, R34, and Y36, are considered as critical for binding to the receptor, since their mutation induces a dramatic drop of activity. Three of these five residues are present in sMTX: K23, N26, and Y32 are equivalent to K27, N30, and Y36 respectively. The two remaining residues are different: I25 in sMTX stands for M29 in CTX and the K30 replaces the R34. Since the effect of these two particular mutations on the pharmacological activity are weak (drop of 1.5 and 3 for M29I and R34K, respectively), it can be supposed that sMTX acts on Kv1.3 in the same way as CTX and K23 in sMTX plays the role of K27 in CTX, protruding in the channel pore. These local differences between the two toxins could explain the weaker activity of sMTX on Kv1.3 channels compared to CTX.

But local similarities (or differences) are not sufficient to fully explain the specificity encountered.[49] Modifications, done on both channel and CTX residues, are somewhat puzzling. The mutation T449F

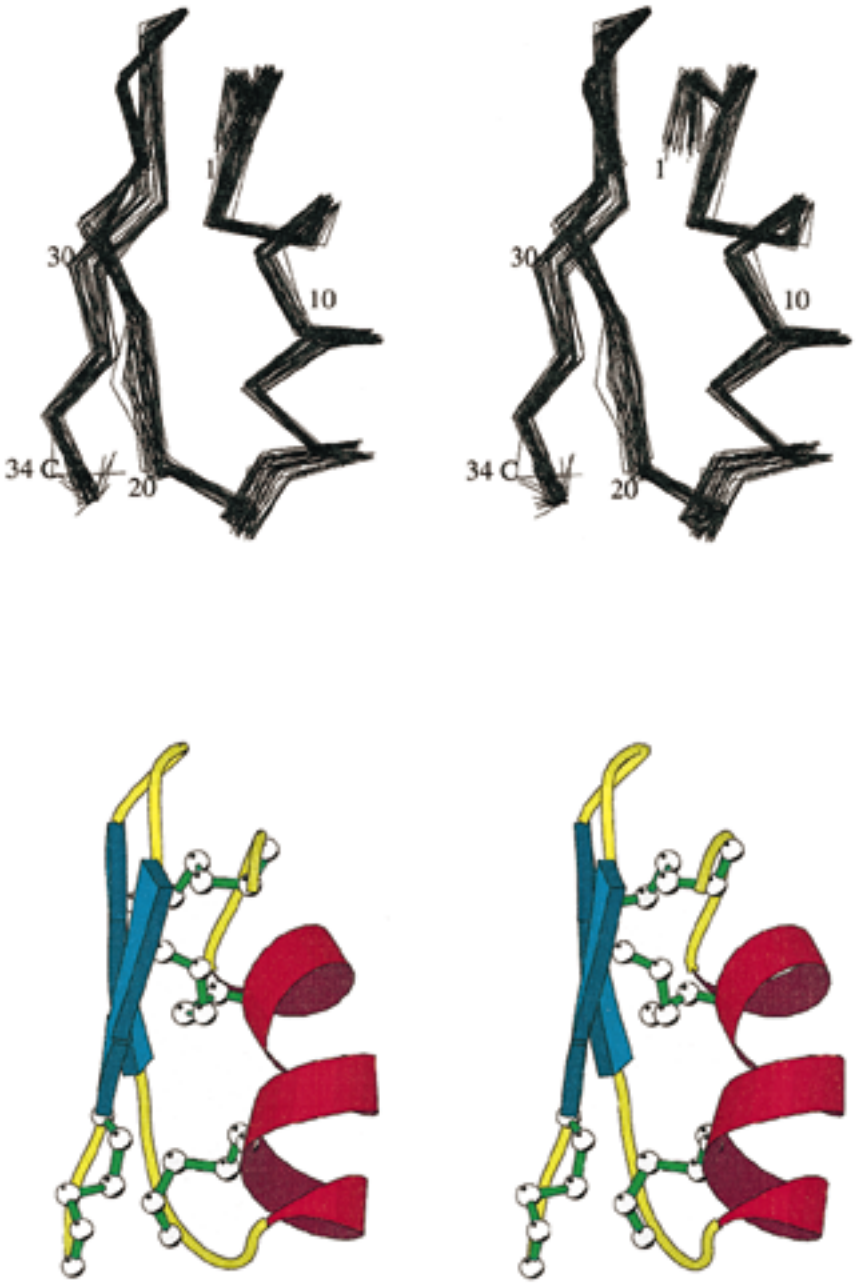

Fig. 6. **Top:** MOLSCRIPT[55] stereo view of the 35 best molecular maurotoxin structures, only the Cα traces are displayed. **Bottom:** Stereo ribbon drawing of the averaged minimized maurotoxin structure with the disulfide bridges represented in balls and sticks.

(H404 in Kv1.3) of the Shaker channel associated with the M29I modification of CTX is highly unfavourable, due to steric hindrance.[50] The Kv1.1 channel has a tyrosine at the equivalent position 404, and sMTX has an isoleucine in place of M29 in CTX, and sMTX blocks Kv1.1 (Kd = 37 nM). In the same idea,

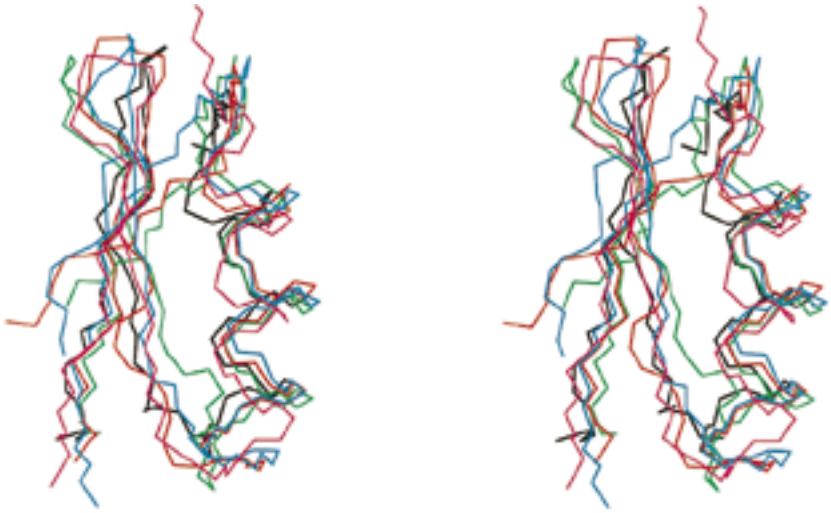

Fig. 7. Stereo view of the maurotoxin backbone in black superposed with the charybdotoxin (PDB code 2crd first structure) in green, noxiustoxin (PDB code 1sxm first structure) in orange, margatoxin (PDB code 1mtx first structure) in blue, and P05 (PDB code 1pnh) in pink.

G380H makes Kv1.3 resistant to KTX, whereas KTX is an effective blocker of Kv1.1, which has a histidine at this position and G380Q renders Kv1.3 resistant to CTX, a blocker of Kv1.2, which has a glutamine at this position.[16] In order to solve this puzzle, we investigated the electrostatic characteristics of both sMTX and the Kv1.2 channel, and for that, built a docking model of this complex.

Previous studies on scorpion toxins acting on voltage-gated potassium channels[16,51,52] allowed to characterise the binding site between the toxin and its receptor. The Kv channels are composed of N- and C-terminal cytoplasmic fragments of varying lengths, and of six membrane-spanning domains S1 to S6. The loop connecting S5 to S6, which is the pore-forming region, has been identified as being the target of scorpion toxins. A three-dimensional model of this region, derived from scorpion toxin studies has been constructed.[16] We modeled the Kv1.2 pore region according to this Kv1.3 model and calculated its charge anisotropy. The resulting dipole moment is oriented along the symmetry axis, due to the fourfold symmetry of the homotetramer, and is oriented from the outer to the inner side of the membrane. We calculated the sMTX dipole moment as well, and analyzed the toxin/receptor docking, assuming that the charge anisotropy is the driving force of the interaction, and thus leads to alignment of the two dipole moments. The orientation of the toxin is such that sMTX presents its K23 to the center of the Kv1.2 pore, interacting electrostatically with a ring of four acidic residues, the D402 from the four symmetric subunits (Fig. 8). A rotation of the toxin around the axis of the dipole and around the central K23, orients the K27 residue close to D386 (subunit C). These two residues K23 and K27 are homologous to K27 and R31 in KTX, respectively, and sMTX could be oriented relative to Kv1.2 in the same way as KTX relative to Kv1.3. Such an orientation has been described for the KTX/Kv1.3, and CTX/Kv1.3 complexes. We checked the orientation of the dipole moments for these two toxins and noticed that they are also directed to the center of the pore. Our resulting docking model further shows a network of possible interactions between sMTX and the Kv1.2 channel. These are composed of, in the first place by a hydrophobic cluster formed between the residues I25, Y32 on the toxin, and V404 (subunits C and D) and V393 (subunit C) on the receptor. Furthermore, there could be an electrostatic bond between K7 (toxin) and D386 (subunit A receptor) and a hydrogen bond between the side chains of N26 (toxin) and T406 (subunit C receptor).

We came to the conclusion that the explanation of the specificity of the interaction of the toxin with its receptor site needs to take into account the whole charge repartition on the toxin. This could explain that modifications of some residues of CTX,[48] far away from the interacting surface CTX/Shaker, such as S10, modify the binding capacity of the toxin (drop of activity of 1500 for S10D), while the replacement of residues V4 or N5 by acidic residues (N4D, V5E) give contradictory results (Kd ratios of 3.1 and 0.7,

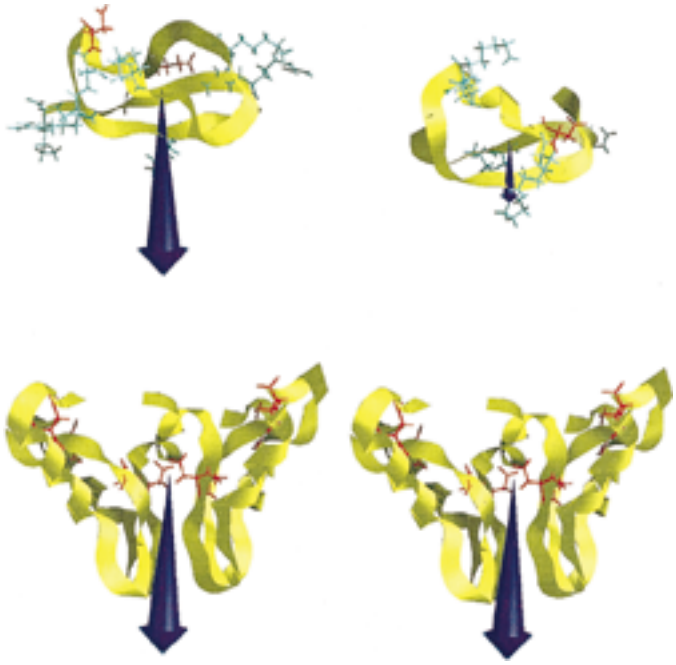

Fig. 8. Schematic representation of the toxin/receptor dipole moments. The left side shows the KTX above the Kv1.2 channel and the right side shows the sMTX above the Kv1.2 channel. Only the backbones are represented (yellow ribbons) with the side chains of charged residues, colored in red (acidic residues) or in blue (basic residues). The arrows indicate the orientation and intensity of the dipole for each molecule.

respectively). As these changes (S10D, N4D, V5E) modify the net charge of the molecule, a variation of the intensity and/or orientation of the dipole moment of the toxin can be expected. Such an approach has also been followed to describe the interaction of fasciculin with achetylcholinesterase.[56,57] These authors had to assume that the charge distribution plays a decisive role in guidance of the ligand toward the achetylcholinesterase. Moreover, using the studies previously performed on the interaction of CTX with BK channels,[14,15,53] and effects of point mutations on the binding efficiency, we tried to understand the drop of activity of sMTX on BK channels compared to CTX. It has been shown that eight residues: S10, W14, R25, K27, M29, N30, R34, and Y36 are crucial for the binding capacity of CTX to the BK channels. The sMTX has equivalent residues for S10, (S6 in sMTX), K27 (K23), N30 (N26), and Y36 (Y32). If the functional map of CTX is respected for sMTX, the orientation of the residues in sMTX can easily be superposed to that of CTX, and the two nonconservative mutations, M29 in CTX replaced by I25 in sMTX, and R25 by N21 may explain the weak activity of sMTX on BK channels.

CONCLUSION

Scorpion toxins are highly active on ionic channels of excitable cells. The short scorpion neurotoxins (29–39 residues) act on potassium channels, while the so-called long neurotoxins (60–70 residues) are specific for sodium channels. These toxins became a useful tool for investigating the channels at a molecular level.[15,16,21,54] Analysis of structure activity relationships of scorpion toxins, leading to the topology of the receptors, enabled to highlight the residues involved in the interaction, and to further understand the general rules of toxin/receptor interactions.

The sequence differences between the members of the voltage-gated potassium channel family are limited. The pore region, which is the toxin binding site, is highly conserved. Thus, understanding the structural basis of the specificity of scorpion toxins for these receptors could lead to the generation of new designed ligands with controled activity and potency. This will be of most importance as the functioning of K channels is involved in numerous physiological functions.

The determination of the sMTX structure showed us that the α/β scorpion toxin scaffold can accommodate, with no major structure modification, another disulfide pairing than those classically observed. The important residues for the recognition of the receptor are present, but we still cannot structurally explain why the sMTX is more active on Kv1.2, than on Kv1.1 and Kv1.3 potassium channels. However, we can speculate that the specificity of scorpion toxins is driven by the overall distribution of ionisable side chains. This charge anisotropy is represented by a dipole moment whose orientation, toward the axis of the pore, is the same for sMTX and for CTX or KTX, but whose intensity is different from one ligand to another. The dipole moment guides and orients the toxin into the pore, toward the binding site and is thus responsible for the specificity. This is supported by the nonexpected results of some point mutations done on CTX. For CTX,[48] only two mutants were more potent to bind to Kv1.3 than the wild-type CTX: V5E and E12Q/K11Q both electrostatic mutants of residues far away from the interacting surface.

ACKNOWLEDGMENTS

E.B. is the recipient of a grant from the Conseil Regional Provence-Alpes Cote d'Azur, France. We thank Dr. Mirjam Czjzek for careful reading of the manuscript, and Dr. Christian Cambillau for constant interest and support.

NOTE ADDED IN PROOF

The solution structure of Pi1 has been published during the publication procedure. This low resolution structure reveals a fold identical to MTX. (Delepiene, M., Prochkina-Chalufour, A,, Possani, L.D. A novel potassium channel blocking toxin from the scorpion pandious imperator: A ^{1}H NMR analysis using a nano-MNR probe. Biochemistry 36:26492658, 1997.)

REFERENCES

1. Chandy, K.G., Gutman, G.A. Voltage-gated K+ channel genes. In: "Handbook of receptors and Channels: Ligand and Voltage-gated Ion Channels." North, A. (ed.). Boca Raton, FL: CRC Press, 1995:1–71.
2. Rader, R.K., Kahn, L.E., Anderson, G.D., Martin, C.L., Chinn, K.S., Gregory, S.A. T cell activation is regulated by voltage-dependent and calcium-activated potassium channels. J. Immunol. 156:1425–1430, 1996.
3. Garcia-Calvo, M., Leonard, R.J., Novick, J., Stevens, S.P., Schmalhofer, W., Kaczorowski, G.J., Garcia, M.L. Purification, characterization, and biosynthesis of margatoxin, a component of *Centruroides margaritatus* venom that selectively inhibits voltage-dependent potassium channels. J. Biol. Chem. 268:18866–18874, 1993.
4. Possani, L.D., Martin, B.M., Sveden, I. The primary structure of noxiustoxin: a K+ channel blocker peptide purified from the venom of the scorpion *Centruroides noxius* Hoffmann. Carlsberg Res. Commun. 47:285–289, 1982.
5. Galvez, A., Gimenez-Gallego, G., Reuben, J.P., Roy-Contancin, L., Feigenbaum, P., Kaczorowski, G.J., Garcia, M.L. Purification and characterization of a unique, potent, peptidyl probe for the high conductance calcium-activated potassium channel from venom of the scorpion *Buthus tamulus*. J. Biol. Chem. 265:11083–11090, 1990.
6. Gimenez-Gallejo, G., Navia, M.A., Reuben, J.P., Katz, G.M., Kaczorowski, G.J., Garcia, M.L. Purification, sequence, and model structure of charybdotoxin, a potent selective inhibitor of calcium-activated potassium channels. Proc. Natl. Acad. Sci. U.S.A. 85:3329–3333, 1988.
7. Garcia, M.L., Garcia-Calvo, M., Hidalgo, P., Lee, A., MacKinnon, R. Purification and characterization of three inhibitors of voltage-dependent K+ channels from *Leiurus quinquestriatus* var. *hebraeus* venom. Biochemistry 33:6834–6839, 1994.
8. Crest, M., Jacquet, G., Gola, M., Zerrouk, H., Benslimane, A., Rochat, H., Mansuelle, P., Martin-Eauclaire, M.-F. Kaliotoxin, a novel peptidyl inhibitor of neuronal BK-type Ca(2+)-activated K+ channels characterized from *Androctonus mauretanicus mauretanicus* venom. J. Biol. Chem. 267:1640–1647, 1992.
9. Zerrouk, H., Mansuelle, P., Benslimane, A., Rochat, H., Martin-Eauclaire, M.-F. Characterization of a new leiurotoxin I-like scorpion toxin. P05 from *Androctonus mauretanicus mauretanicus*. FEBS Lett. 320:189–192, 1993.
10. Chicchi, G.G., Gimenez-Gallejo, G., Ber, E., Garcia, M.L., Winquist, R., Cascieri, M.A. Purification and characterization of a unique, potent inhibitor of apamin binding from *Leiurus quinquestriatus hebraeus* venom. J. Biol. Chem. 263:10192–10197, 1988.
11. Cahalan, M.D. Modification of sodium channel gating in frog myelinated nerve fibres by *Centruroides sculpturatus* scorpion venom. J. Physiol. 244:511–534, 1975.
12. Caterall, W.A. Neurotoxins that act on voltage-sensitive sodium channels in excitable membranes. Annu. Rev. Pharmacol. Toxicol. 20:15–43, 1980.
13. MacKinnon, R., Miller, C. Mutant potassium channels with altered binding of charybdotoxin, a pore-blocking peptide inhibitor. Science 245:1382–1385, 1989.
14. Park, C.-S., Miller, C. Mapping function to structure in a channel-blocking peptide: Electrostatic mutants of charybdotoxin. Biochemistry 31:7749–7755, 1992.
15. Stampe, P., Kolmakova-Partensky, L., Miller, C. Intimations of K+ channel structure from a complete functional map of the molecular surface of charybdotoxin. Biochemistry 33:443–450, 1994.
16. Aiyar, J., Withka, J.M., Rizzi, J.P., Singleton, D.H., Andrews, G.C., Lin, W., Boyd, J., Hanson, D.C., Simon, M., Dethlefs, B., Lee, C.-L., Hall, J.E., Gutman, G.A., Chandy, K.G. Topology of the pore-region of a K+ channel revealed by the NMR-derived structures of scorpion toxins. Neuron 15:1169–1181, 1995.
17. Carbone, E., Wanke, E., Prestipino, G., Possani, L.D., Maelicke, A. Selective blockage of voltage-dependent K+ channels by a novel scorpion toxin. Nature 296:90–91, 1982.
18. Olamendi-Portugal, T., Gòmez-Lagunas, F., Gurrola, G.B., Possani, L. A novel structural class of K+ channel blocking toxin from the scorpion *Pandinus imperator*. Biochem. J. 315:977–981, 1996.
19. Dauplais, M., Gilquin, B., Possani, L.D., Gurrola-Briones, G., Roumestand, C., Menez, A. Determination of the three-dimensional solution structure of noxiustoxin: Analysis of structural differences with related short-chain scorpion toxins. Biochemistry 34:16563–16573, 1995.
20. Bontems, F., Gilquin, B., Roumestand, C. Menez, A., Toma, F. Analysis of side-chain organization on a refined model of charybdotoxin: Structural and functional implications. Biochemistry 31:7756–7764, 1992.
21. Krezel, A.M., Kasibhatla, C., Hidalgo, P., MacKinnon, R., Wagner, G. Solution structure of the potassium channel inhibitor agitoxin 2: Caliper for probing channel geometry. Protein Sci. 4:1478–1489, 1995.
22. Johnson, B.A., Scott, P.S., Williamson, J.M. Determination of the three-dimensional structure of margatoxin by 1H, 13C, 15N triple-resonance nuclear magnetic resonance spectroscopy. Biochemistry 33:15061–15070, 1994.
23. Piantini, U., Sørensen, O.W., Ernst, R.R. Multiple quan-

tum filters for elucidating NMR coupling networks. J. Am. Chem. Soc. 104:6800–6801, 1982.
24. Derome, A.E., Williamson, M.P. Rapid-pulsing artifacts in double-quantum-filtered COSY. J. Magn. Reson. 88:177–185, 1990.
25. Marion, D., Wüthrich, K. Application of phase sensitive two dimensional correlated spectroscopy (COSY) for measurements of H-H spin-spin coupling constants in proteins. Biochem. Biophys. Res. Commun. 113:967–974, 1983.
26. Griesinger, C., Otting, G., Wüthrich, K., Ernst, R.R. Clean-TOCSY for 1H spin system identification in macromolecules. J. Am. Chem. Soc. 110:7870–7872, 1988.
27. Bax, A., Davis, D.G. MLEV-17-based two-dimensional homonuclear magnetization transfer spectroscopy. J. Magn. Reson. 65:355–360, 1985.
28. Kumar, A., Ernst, R.R., Wüthrich, K. A two-dimensional nuclear Overhauser enhancement (2D nOe) experiment for the elucidation of complete proton-proton cross-relaxation networks in biological macromolecules. Biochem. Biophys. Res. Commun. 95:1–6, 1981.
29. Delaglio, F., Grzesiek, S., Vuister, G.W., Zhu, G., Pfeifer, J., Bax, A. NMRPipe: A multidimensional spectral processing system based on UNIX pipes. J. Biomol. NMR 6:277–293, 1995.
30. Wüthrich, K. "NMR of Protein and Nucleic Acids." New York: Wiley, 1986.
31. Eccles, C., Güntert, P., Billeter, M., Wüthrich, K. Efficient analysis of protein 2D NMR spectra using the software package EASY. J. Biomol. NMR 1:111–130, 1991.
32. Güntert, P., Braun, W., Wüthrich, K. Efficient computation of three-dimensional protein structures in solution from NMR data using the program DIANA and the supporting programs CALIBA, HABAS and GLOMSA. J. Mol. Biol. 217:517–530, 1991.
33. Güntert, P., Wüthrich, K. Improved efficiency of protein structure calculations from NMR data using the program DIANA with redundant dihedral angle constraints. J. Biomol. NMR 1:447–456, 1991.
34. Brünger, A.T. X-PLOR v3.1 Manual. New Haven, CT: Yale University, 1992.
35. Nicholls, A., Sharp, K.A., Honig, B. Protein folding and association: Insights from the interfacial and thermodynamic properties of hydrocarbons. Proteins 11:281–296, 1991.
36. Nicholls, A., Honig, B. A rapid finite difference algorithm, utilizing successive over-relaxation to solve the Poisson-Boltzmann equation. J. Comp. Chem. 12:435–445, 1991.
37. Roussel, A., Cambillau, C. "Silicon Graphics Geometry Partner Directory." Mountain View, CA: Silicon Graphics, 1989:77–78.
38. Laskowski, R.A., MacArthur, M.W., Moss, D.M., Thornton, J.M. PROCHECK: A program to check the stereochemical quality of protein structures. J. Appl. Crystallogr. 26:283–291, 1993.
39. Wishart, D.S., Sykes, B.D., Richards, F.M. The chemical shift index: A fast and simple method for the assignment of protein secondary structure through NMR spectroscopy. Biochemistry 31:1647–1651, 1992.
40. Szyperski, T., Güntert, P., Otting, G., Wüthrich, K. Determination of scalar coupling constants by inverse Fourier transformation of in-phase multiplets. J. Magn. Reson. 99:552–560, 1992.
41. Widmer, H., Wüthrich, K. Simulated two-dimensional NMR cross-peak fine structures for 1H spin systems in polypeptides and polydeoxynucleotides. J. Magn. Reson. 74:316–336, 1987.
42. Richardson, J.S. The anatomy and taxonomy of protein structure. Adv. Protein Chem. 34:167–339, 1981.
43. Bontems, F., Roumestand, C., Gilquin, B., Menez, A., Toma, F. Refined structure of charybdotoxin: Common motifs in scorpion toxins and insect defensins. Science 254:1521–1523, 1991.
44. Meunier, S., Bernassau, J.M., Sabatier, J.M., Martin-Eauclaire, M.F., Van Rietschoten, J., Cambillau, C., Darbon, H. Solution structure of P05-NH2, a scorpion toxin with high affinity for apamin-sensitive K+ channel. Biochemistry 32:11969–11976, 1993.
45. Bontems, F., Roumestand, C., Boyot, P., Gilquin, B., Doljansky, Y., Menez, A., Toma, F. Three-dimensional structure of natural charybdotoxin in aqueous solution by 1H-NMR: Charybdotoxin possesses a structural motif found in other scorpion toxins. Eur. J. Biochem. 196:19–28, 1991.
46. Johnson, B.A., Sugg, E.E. Determination of the three-dimensional structure of iberiotoxin in solution by 1H nuclear magnetic resonance spectroscopy. Biochemistry 31:8151–8159, 1992.
47. Blanc, E., Fremont, V., Sizun, P., Meunier, S., Van Rietschoten, J., Thevand, A., Bernassau, J.M., Darbon, H. Solution structure of P01, a natural scorpion peptide structurally analogous to scorpion toxins specific for apamin-sensitive potassium channel. Proteins 24:359–369, 1996.
48. Goldstein, S.A.N., Pheasant, D.J., Miller, C. The charybdotoxin receptor of a shaker K+ channel: Peptide and channel residues mediating molecular recognition. Neuron 12: 1377–1388, 1994.
49. Goldstein, S.A.N., Colatsky, T.J. Ion channels: Too complex for drug design? Meeting review. Neuron 16:913, 919, 1996.
50. Naranjo, D., Miller, C. A strongly interacting pair of residues on the contact surface of charybdotoxin and a shaker channel. Neuron 16:123–130, 1996.
51. Lipkind, G.M., Hanck, D.A., Fozzard, H.A. A structural motif for the voltage-gated potassium channel pore. Proc. Natl. Acad. Sci. U.S.A. 92:9215–9219, 1995.
52. Grissmer, S., Nguyen, A.N., Aiyar, J., Hanson, D.C., Mather, R.J., Gutman, G.A., Karmilowicz, M.J., Auperin, D.D., Chandy, G. Pharmacological characterization of five cloned voltage-gated K+ channels, types Kv1.1, 1.2, 1.3, 1.5, and 3.1, stably expressed in mammalian cell lines. Mol. Pharmacol. 45:1227–1234, 1994.
53. Munujos, P., Knaus, H.-G., Kaczorowski, G.J., Garcia, M. Cross-linking of charybdotoxin to high-conductance calcium-activated potassium channels: Identification of the covalently modified toxin residue. Biochemistry 34:10771–10776, 1995.
54. Naini, A.A., Miller, C. A symmetry-driven search for electrostatic interaction partners in charybdotoxin and a voltage-gated K+ channel. Biochemistry 35:6181–6187, 1996.
55. Kraulis, P.J. MOLSCRIPT: A program to produce both detailed and schematic plots of protein structures. J. Appl. Crystallogr. 24:946–950, 1991.
56. Van den Born, H.K.L., Radic, Z., Marchot, P., Taylor, P., Tsigelny I. Theoretical analysis of the structure of the peptide facsiculin and its docking to achetylcholinesterase. Protein Sci. 4:703–715, 1995.
57. Bourne, Y., Taylor, P., Marchot, P. Acetylcholinesterase inhibition by fasciculin: Crystal structure of the complex. Cell 83:503–512, 1995.
58. Kharrat, R., Mansvelle, P., Sampieri, F., Crest, M., Martin-Eauclaire, M.F., Rochat, M., El Ayeb, M. Maurotoxin, a new four disulfide bridges toxin from Scorpio maurus venom: purification structure and pharmacology on potassium channels. FEBS letters 406:284–290, 1997.
59. Kharrat, R., Mabrouk, K., Crest, M., Dorbon, H., Oughuideni, R., Martin-Eauclaire, M.F., Jacquet, G., El Ayeb, M., Van Rietschoten J., Rochat, M., Sampien, J.M. Chemical synthesis and characterisation of maurotoxin, a short scorpion toxin with four disulfide bridges that acts on k^+ channels. Eur. J. Biochem 242:491–498, 1996.